Application of the discrete dipole approximation to very large refractive indices: Filtered coupled dipoles revived

Yurkin, M.A.; Min, M.; Hoekstra, A.G.

Published in:
Physical Review E

DOI:
10.1103/PhysRevE.82.036703

Application of the discrete dipole approximation to very large refractive indices: Filtered coupled dipoles revived

Maxim A. Yurkin,[1,2,*] Michiel Min,[3] and Alfons G. Hoekstra[4]
[1]*Institute of Chemical Kinetics and Combustion, Institutskaya 3, Novosibirsk 630090, Russia*
[2]*Novosibirsk State University, Pirogova 2, Novosibirsk 630090, Russia*
[3]*Astronomical Institute Utrecht, Princetonplein 5, 3584 CC Utrecht, The Netherlands*
[4]*Computational Science Research Group, Faculty of Science, University of Amsterdam, Science Park 107, 1098 XG Amsterdam, The Netherlands*
(Received 31 May 2010; published 27 September 2010)

We compared three formulations of the discrete dipole approximation (DDA) for simulation of light scattering by particles with refractive indices $m=10+10i$, $0.1+i$, and $1.6+0.01i$. These formulations include the filtered coupled dipoles (FCD), the lattice dispersion relation (LDR) and the radiative reaction correction. We compared the number of iterations required for the convergence of the iterative solver (proportional to simulation time) and the accuracy of final results. We showed that the LDR performance for $m=10+10i$ is especially bad, while the FCD is a good option for all cases studied. Moreover, we analyzed the detailed structure of DDA errors and the spectrum of the DDA interaction matrix to understand the performance of the FCD. In particular, this spectrum, obtained with the FCD for particles smaller than the wavelength, falls into the bounds, physically implied for the spectrum of the infinite-dimensional integral scattering operator, contrary to two other DDA formulations. Finally, such extreme refractive indices can now be routinely simulated using modern desktop computers using the publicly available ADDA code, which includes an efficient implementation of the FCD.

DOI: 10.1103/PhysRevE.82.036703 PACS number(s): 02.70.−c, 42.25.Fx, 42.68.Mj

I. INTRODUCTION

The discrete dipole approximation (DDA) is a well-known method to calculate light scattering by arbitrary shaped inhomogeneous particles [1]. The widespread application of the DDA started with the work of Draine and coworkers [2–4]. They showed that DDA accuracy decreases and computational time increases with increasing refractive index m. Based on those studies it was commonly accepted that application of the DDA is limited to a range approximately described as $|m-1|<2$, assuming the standard formulation of the DDA including the lattice dispersion relation (LDR [2]). However, DDA performance changes smoothly with increasing m, so this criterion should be considered only as a practical guideline. Recently, it has been shown that this standard DDA formulation has similar problems both for $|m|\gg 1$ and $\mathrm{Re}(m)\ll 1$ [5]. Such "extreme" (we will further use this term) m-values do appear in spectral resonances of many materials in the infrared range [5] (see Fig. 1 [6–9]). Accurate predictions of the spectral shape of absorption resonances are of crucial importance for the interpretation of astronomical observations. Moreover, metallic particles in the infrared have very large values of m, hence they might be the dominant source of opacity in many environments [10]. However, currently accurate methods to predict the opacity of metallic particles with complex shape and size comparable to or smaller than the wavelength are lacking.

While the range of $\mathrm{Re}(m)<1$ is poorly studied with regards to comparing different DDA formulations, there have been a number of attempts to improve DDA performance for large m. These attempts include the filtered coupled dipoles (FCD [11]), the weighted discretization (WD [12]), the integration of Green's tensor (IT [13]), the Rahmani–Chaumet–Bryant formulation (RCB [14,15]), and the surface-corrected LDR (SCLDR [16]). The RCB and the SCLDR require a preliminary solution of the electrostatic problem (i.e., in the long-wavelength limit) for the particle of the same shape. The IT requires a numerical evaluation of oscillatory integrals to build up the DDA interaction matrix, which is not trivial to implement and may consume a lot of computer time. The WD is efficient in decreasing shape errors [17] but

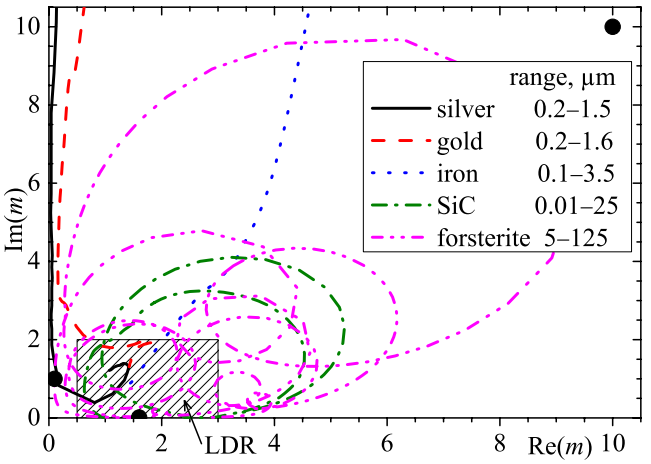

FIG. 1. (Color online) Refractive indices of noble metals and typical constituents of astrophysical dust in and around the visible wavelength range, depicted in the complex plane. A shaded region schematically shows the known range of LDR applicability. Three dots denote refractive indices examined in this paper.

*Corresponding author; yurkin@gmail.com

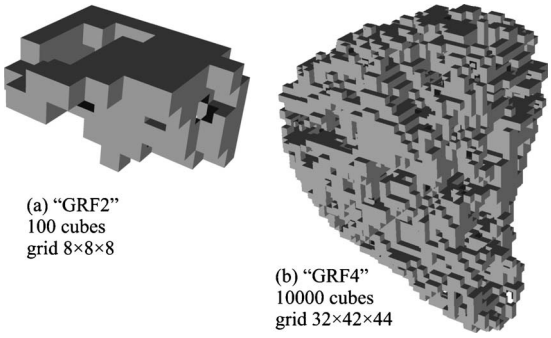

FIG. 2. Particles GRF2 (a) and GRF4 (b), obtained by cubical discretization of the Gaussian random field. Images were generated with LITEBIL v.0.9.5b [38].

it causes all boundary dipoles to have different polarizabilities, which is incompatible with current internal data structure of publicly available DDA codes such as DDSCAT [4] and ADDA [18]. For the FCD the only known drawback is difficulties in theoretical analysis of its convergence [17]. On the other hand, the FCD is easy to implement and it does improve the performance of the DDA for large m, as was shown by its authors [11,19]. It seems that the only reason why the FCD, proposed 10 years ago, was not adopted by the light scattering community is that so far it was not included in a publicly available DDA code.

In this paper we endeavor to revive the FCD. For that we implement it in the ADDA code and demonstrate its performance for a number of scattering problems in comparison with the LDR and the radiative reaction correction (RR [3]) formulations. We also discuss practical feasibility of DDA simulation of light scattering by particles with extreme refractive indices. To understand the reasons for difference in performance between different DDA formulations and particle shapes, we analyze the detailed structure of DDA errors and the spectrum of the DDA interaction matrix.

Preliminary results of this paper were presented earlier at the 11th Conference on Electromagnetic and Light Scattering [20]. Moreover, in a recently published paper [21] the performance of the FCD was studied specifically for gold nanoparticles.

II. METHODS

A. Test scatterers

We tried three values of m: $10+10i$, $0.1+i$, $1.6+0.01i$ (Fig. 1) The first two values are extreme and typical for SiC in the infrared, the second one is also typical for noble metals. The third value, a moderate one, is typical for silicates in the visible part of the spectrum. The following shapes were used: a sphere, a cube, and Gaussian random field particles (GRF [22]). For the latter two cubical discretizations were employed, using 10^2 and 10^4 elements and denoted by GRF2 and GRF4, respectively (Fig. 2). We used two different sizes: $kD_x=8$ ("large") and $kD_x=10^{-5}$ (Rayleigh regime), where k is the wave number and D_x is the particle length along the x axis. For both cases orientation of the particle was fixed. We used the FCD, LDR, and RR formulations for the large particles. For the Rayleigh particles the LDR and the RR are both equivalent to the classical Clausius-Mossotti (CM)—so only the FCD and the CM were used.

For each combination of shape, size, and refractive index we used 18 different discretizations from 8 to 512 dipoles (n_x) per D_x with approximately uniform spacing on a logarithmic scale. The lower bound of n_x is determined by adequacy of the discrete representation of the shape, and the upper bound—by acceptable computational requirements. The only exception is GRF4 particle, initial description of which has $n_x=31$. For this particle we used 8 values of n_x from 31 to 434 (initial value and that multiplied by even numbers up to 14). We also tried odd multiples of the initial n_x but they resulted in a separate convergence curve (data not shown). In other words, the convergence of measured quantities with increasing n_x was smooth and to the same values both for even and odd multiples, when they are considered separately. However, there is significant difference between results for adjacent even and odd multiples. This behavior, especially prominent for the FCD and extreme m, warrants a separate study, so we do not consider results for the GRF4 and odd multiples of $n_x=31$ in this paper.

B. DDA formulations

We start with a short excerpt from the derivation of the DDA starting from the volume-integral equation for the electric field [1]. One of the possible forms of the latter is

$$\mathbf{E}(\mathbf{r}) = \mathbf{E}^{\mathrm{inc}}(\mathbf{r}) + \mathrm{p.v.}\int \mathrm{d}^3 r' \bar{\mathbf{G}}(\mathbf{r},\mathbf{r}')\chi(\mathbf{r}')\mathbf{E}(\mathbf{r}') - \frac{4\pi}{3}\chi(\mathbf{r})\mathbf{E}(\mathbf{r}), \quad (1)$$

where $\mathbf{E}^{\mathrm{inc}}$ and $\mathbf{E}$ are the incident and total electric field, and $\chi(\mathbf{r})=[\varepsilon(\mathbf{r})-1]/4\pi$ is the electric susceptibility ($\varepsilon=m^2$—relative permittivity). In this paper only isotropic materials are considered. $\chi(\mathbf{r})$ vanishes outside the volume of the particle, therefore integration can be considered over the whole space. p.v. denotes the principal value of the integral, which corresponds to exclusion of infinitesimal sphere around point $\mathbf{r}$. The free-space Green's tensor is the following:

$$\bar{\mathbf{G}}(\mathbf{r},\mathbf{r}') = \frac{\exp(\mathrm{i}kR)}{R}\left[k^2\left(\bar{\mathbf{I}} - \frac{\hat{R}\hat{R}}{R^2}\right) - \frac{1-\mathrm{i}kR}{R^2}\left(\bar{\mathbf{I}} - 3\frac{\hat{R}\hat{R}}{R^2}\right)\right], \quad (2)$$

where k is the free-space wave vector, $\mathbf{R}=\mathbf{r}-\mathbf{r}'$, $R=|\mathbf{R}|$, $\bar{\mathbf{I}}$ is the identity tensor, and $\hat{R}\hat{R}$ is a tensor defined as $\hat{R}\hat{R}_{\mu\nu}=R_\mu R_\nu$.

Standard DDA formulations are obtained by dividing the volume of the particle into equal cubical cells V_i (dipoles) and using stepwise approximation for both $\chi(\mathbf{r}')\mathbf{E}(\mathbf{r}')$ and $\bar{\mathbf{G}}(\mathbf{r},\mathbf{r}')$ under the integral. Then Eq. (1) is considered in all dipole centers ($\mathbf{r}=\mathbf{r}_i$), and the integral over the self-cell is evaluated using another (not stepwise) approximation,

$$\text{p.v.}\int_{V_i} \mathrm{d}^3 r' \bar{\mathbf{G}}(\mathbf{r}_i,\mathbf{r}')\chi(\mathbf{r}')\mathbf{E}(\mathbf{r}') = M_i\chi_i\mathbf{E}_i, \tag{3}$$

where $\chi_i=\chi(\mathbf{r}_i)$ and $\mathbf{E}_i=\mathbf{E}(\mathbf{r}_i)$. Three standard DDA formulations (CM, RR, and LDR) considered in this paper differ only by the values of self-induction term M_i,

$$M^{\mathrm{CM}} = 0, \quad M^{\mathrm{RR}} = \frac{2}{3}ix^3,$$

$$M^{\mathrm{LDR}} = (b_1 + b_2 m^2 + b_3 m^2 S)x^2 + \frac{2}{3}ix^3, \tag{4}$$

where $x=kd$ is the size parameter of a dipole (d—dipole size), b_1-b_3 are numerical constants, and S depends on the polarization of the incident light. The details of the latter, as well as motivation behind expressions in Eq. (4) can be found in [1]. It is convenient to define dipole polarization $\mathbf{P}_i=V\chi_i\mathbf{E}_i$ and polarizability $\alpha_i=V\chi_i[1+(4\pi/3-M_i)\chi_i]^{-1}$, where V is the volume of one dipole. Then the main DDA equations can be formulated as

$$\alpha_i^{-1}\mathbf{P}_i - \sum_{j\neq i}\bar{\mathbf{G}}_{ij}\mathbf{P}_j = \mathbf{E}_i^{\mathrm{inc}}, \tag{5}$$

where $\mathbf{E}_i^{\mathrm{inc}}=\mathbf{E}^{\mathrm{inc}}(\mathbf{r}_i)$ and $\bar{\mathbf{G}}_{ij}=\bar{\mathbf{G}}(\mathbf{r}_i,\mathbf{r}_j)$. This system of linear equations is solved for $\mathbf{P}_i$, which is further used to calculate any measured quantities [1].

The FCD is based on the sampling theorem, applied to the product $\chi\mathbf{E}$ [11],

$$\chi(\mathbf{r})\mathbf{E}(\mathbf{r}) \approx V\sum_i \chi_i\mathbf{E}_i h_{\mathrm{r}}(\mathbf{r}-\mathbf{r}_i), \tag{6}$$

where $h_{\mathrm{r}}(\mathbf{R})=h_{\mathrm{r}}(R)=[\sin(k_{\mathrm{F}}R)-k_{\mathrm{F}}R\cos(k_{\mathrm{F}}R)]/(2\pi^2R^3)$ is the impulse response function of the ideal antialiasing filter that suppresses all spatial spectral components outside the sphere with radius $k_{\mathrm{F}}=\pi/d$. Equation (6) becomes exact if the spatial Fourier spectrum of $\chi\mathbf{E}$ is bounded inside this sphere.

Piller and Martin [11] showed that the spectrum of $\mathbf{E}$ inside any homogeneous particle with *real* refractive index m lies on a sphere with radius km. This statement is based on expansion of $\mathbf{E}$ into appropriate regular basis (Bessel multipoles) inside the particle and continuation of this expansion to the whole space, ignoring the particle boundary. The latter is fine for solution of Eq. (1) inside the particle, since χ anyway vanishes outside. However, it is at least hard to extend this property either to multidomain scatterers or to complex m. Moreover, although the maximum of the spectrum of χ is at the origin, this spectrum always extends to infinity, since support of χ is finite. To alleviate the latter preliminary filtering of χ was proposed [11], which distorts χ (i.e., the original particle is replaced by one with a smoothed boundary), but improves the accuracy of Eq. (6). The optimum strategy for filtering χ is yet to be found, however, there seem to be little difference between several tested options [11]. In this paper we employ no filtering of χ, because it is incompatible with current internal data structure of ADDA (see also remark concerning the WD in Sec. I).

The remarkable property of the FCD is that Eq. (6) is the only approximation used. After substituting it into Eq. (1) the Green's tensor can be analytically integrated with $h_{\mathrm{r}}(\mathrm{R})$, leading to the filtered Green's tensor [23],

$$\bar{\mathbf{G}}^{\mathrm{F}}(\mathbf{r},\mathbf{r}') = \bar{\mathbf{G}}^{\mathrm{F}}(\mathbf{R}) = \bar{\mathbf{I}}\left(k^2 g_{\mathrm{F}}(R) + \frac{g_{\mathrm{F}}'(R)}{R} + \frac{4\pi}{3}h_{\mathrm{r}}(R)\right) + \frac{\hat{R}\hat{R}}{R^2}\left(g_{\mathrm{F}}''(R) - \frac{g_{\mathrm{F}}'(R)}{R}\right), \tag{7}$$

$$g_{\mathrm{F}}(R) = \frac{\sin(kR)[\pi i + C^- - C^+] + \cos(kR)[S^+ + S^-]}{\pi R},$$

$$\left\{\begin{array}{l} C^{\pm} = \mathrm{Ci}[(k_{\mathrm{F}} \pm k)R] \\ S^{\pm} = \mathrm{Si}[(k_{\mathrm{F}} \pm k)R] \end{array}\right\}. \tag{8}$$

We note that Eqs. (7) and (8) differ by a factor of 4π from the original expressions [11,23], which is compensated by use of χ instead of $\Delta\varepsilon=\varepsilon-1$. Moreover, the expression for $g_{\mathrm{F}}(\mathrm{R})$ given in [11] contained an error—$\sin(kR)$ and $\cos(kR)$ were interchanged, and so were C^+ and C^-. However, this was corrected in a later publication by the same group [23]. The FCD requires $k_{\mathrm{F}}>k$, i.e., $d<\lambda/2$, but application of the DDA outside this domain has little sense anyway.

Another consequence of filtering is that $\bar{\mathbf{G}}^{\mathrm{F}}(\mathbf{R})$ is no more singular for zero argument, allowing exact evaluation of the self-term. We provide an explicit expression for the latter as it was not given in the original papers [11,23],

$$\bar{\mathbf{I}}M^{\mathrm{FCD}} = V\lim_{R\to 0}\bar{\mathbf{G}}^{\mathrm{F}}(\mathbf{R}), \quad M^{\mathrm{FCD}} = \frac{4}{3}x^2 + \frac{2}{3}\left(i + \frac{1}{\pi}\ln\frac{\pi-x}{\pi+x}\right)x^3. \tag{9}$$

The final DDA equations for the FCD are the same as Eq. (5), but with $\bar{\mathbf{G}}_{ij}=\bar{\mathbf{G}}^{\mathrm{F}}(\mathbf{r}_i,\mathbf{r}_j)$ and α calculated using M^{FCD} from Eq. (9). We also note that compared to standard DDA formulations the FCD incurs additional computational overhead for evaluating sine and cosine integrals to build-up the interaction matrix. However, according to our experience, this one-time overhead is comparable to a single iteration of the iterative solver and hence can be neglected in most cases (data not shown).

C. Details of DDA simulations

We have implemented the FCD (without filtering of susceptibility) in ADDA and used it (v.0.78.2 [24]) for all simulations presented in this paper. We used the QMR iterative solver [18] for all simulations, except a few cases, in which the BiCGStab was used (see below). For refractive indices $10+10i$ and $0.1+i$ we employed the default threshold of the iterative solver (10^{-5}), but for $1.6+0.01i$ we set it to 10^{-10} to preclude its influence on the accuracy results. For large and Rayleigh particles we use $y=kd|m|$ and $1/n_x$ as discretization parameters, respectively. For spheres we employed volume correction (a default option in ADDA), which ensures that the dipole discretization of the particle has the correct volume [18]. All simulations were run on the Dutch compute cluster LISA [25].

To compute all measured quantities, e.g., the Mueller scattering matrix, one generally has to consider two polarizations of the incident wave. But if a particle has a fourth order rotation axis coincident with the incident propagation direction, ADDA simulates only one polarization [18], decreasing simulation time twofold. In the following we present data on number of iterations and computational time for a *single* polarization of the incident wave to adequately compare symmetric and nonsymmetric shapes.

To facilitate further discussion we adopt several definitions from [17,26]. *Cubically* (*noncubically*) *shaped* particles are those that can (cannot) be exactly described by a set of cubical subvolumes. The *shape error* (present only for noncubically shaped particles) is the difference between some measured quantity for a discretized particle shape (calculated to a high accuracy) and that for the original shape. This type of errors does not depend on a particular DDA formulation, but only on the geometry of the discretization. The *discretization error* is the difference between the result obtained using a limited number of dipoles and an exact (very accurate) solution for the cubical discretization of the particle. The *surface error* is a part of the discretization error, which converges linearly with y (or d). The remaining part converges quadratically with y. Moreover, surface errors appear due to the particle interface and they are expected to increase with increasing surface-to-volume ratio of the particle [17]. In the current paper the spheres are the only noncubically shaped particles that have shape errors. Among other shapes the GRF4 particles are expected to have the largest surface errors.

D. Extrapolation technique

Since only the sphere allows for exact analytical solution, we used the extrapolation technique based on results for 5 best discretizations [26] to infer reference results for the cube and the GRF particles. In a single case, the GRF4 particle with $m=10+10i$ using the LDR, extrapolation was based on results of only four discretizations due to convergence failures for other values of y [see Fig. 6(b)]. Using error estimates provided by the extrapolation technique for all DDA formulations applied to the same particle and assuming these errors to be independent, we computed a weighted average (μ) of extrapolation results and its error estimate (σ). Then we computed the corrected error estimates for each formulation as $\sigma_x^2=(x-\mu)^2+\sigma^2$, where x is extrapolation result.

For spheres we also performed extrapolation (using results for nine best discretizations) to compare its accuracy relative to the exact Mie results. The results of this comparison (real errors) will be presented below, while the internal estimate of the extrapolation error in most cases was adequate in describing (i.e., was larger than) the real errors (data not shown). The only exception occurred for large spheres with $m=10+10i$, for which the estimate was three to eight times smaller than the real errors.

The extrapolation technique was also used to compute accurate results for different cubical discretizations of a sphere, which allowed us to separate shape and discretization errors as described in [26]. Cubical discretizations were obtained using $n_x=8$, 16, 24, 32, 48, and 64. Further these shapes were described with several refined grids (n_x up to 640) and light scattering was simulated using the FCD for $m=10+10i$ and $1.6+0.01i$, and the RR for $m=0.1+i$.

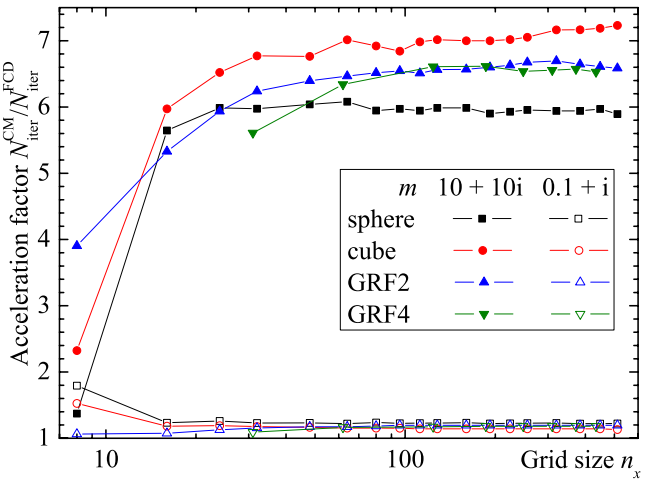

FIG. 3. (Color online) Ratio of number of iterations when using FCD and CM formulations for Rayleigh particles with $m=10+10i$ and $0.1+i$ versus the grid size.

III. RESULTS OF THE DDA SIMULATIONS

A. Convergence of the iterative solver

We start by analyzing the number of iterations (N_{iter}) of the iteration method, which is the main factor determining total simulation time. For Rayleigh particles FCD is faster than CM for both extreme refractive indices, while N_{iter} is only weakly dependent on the discretization (Fig. 3). Acceleration from employing the FCD is approximately 6 and 1.2 times for $m=10+10i$ and $0.1+i$ respectively, which is in line with literature data for slightly different problem parameters [19]. Results of N_{iter} for both particle sizes, but for a single discretization level $n_x=128$ (124 for the GRF4), are presented in Table I. For large particles with any of the considered m, as well as for Rayleigh particles with $m=1.6+0.01i$, all formulations show very similar N_{iter} almost independent on y, except for the following two peculiarities.

First, for $m=10+10i$ the LDR shows strongly nonmonotonic dependence of N_{iter} on y for all studied shapes (see Fig. 4 for example). This can be explained by the nature of the LDR formulation, which employs corrections of order y^2 [Eq. (4)]. When y is not small this correction may be large and wrong, which not only decreases the accuracy of the simulations (see below) but also strongly increases the condition number of the interaction matrix. This is not so noticeable for very coarse discretizations due to the small dimension of the interaction matrix, but becomes prominent for $y\sim 1$. Other formulations employ corrections given in powers of x [Eqs. (4) and (9)], which is much smaller than y for this m. It is important to note that when the LDR is faster than other formulations ($y>1$), it leads to huge errors (see below) that preclude any practical application.

Second, the QMR iterative solver fails for very fine discretizations of cubes for both the RR and the LDR and for

TABLE I. Number of iterations for a single run of QMR iterative solver when $n_x=128$ (or 124).

		$kD_x \ll 1$		$kD_x=8$		
m	Shape	CM	FCD	RR	LDR	FCD
$10+10i$	Sphere	431	72	1644	6122	1457
	Cube	428	61	1257[a]	>30000 [a]	1496[a]
	GRF2	571	87	1251	27693	1133
	GRF4	608	92	1257	>30000	1208
$0.1+i$	Sphere	112	91	189	188	159
	Cube	121	106	155[a]	149[a]	144[a]
	GRF2	129	108	176	175	161
	GRF4	130	111	173	173	167
$1.6+0.01i$ [b]	Sphere	15	14	66	67	63
	Cube	15	14	96	96	95
	GRF2	17	15	39	39	38
	GRF4	17	15	35	35	35

[a]BiCGStab iterative solver was used.
[b]For this m we used convergence threshold of the iterative solver equal to 10^{-10}, therefore shown values of N_{iter} are approximately twice as large as for the default threshold of 10^{-5}.

both extreme refractive indices (data not shown). We leave this fact for a future study and use the BiCGStab in these cases. The latter works fine and leads to reasonable N_{iter} for all DDA formulations except for the LDR in combination with $m=10+10i$ (see Table I).

Piller [19] showed that for refractive indices close to the real axis acceleration by using the FCD may be even larger than shown above. We performed only a single test to confirm that (a sphere, $m=5$, $n_x=16$, $kD_x=10^{-5}$), resulting in N_{iter} equal to 22 and 680 for the FCD and the CM respectively (acceleration factor of 31).

B. Accuracy of absorption cross section

In this paper, we show and analyze the accuracy results only for the absorption cross section (C_{abs}) for fixed propagation direction and polarization of the incident wave (along the z and y axes, respectively). Accuracy of other quantities, such as extinction cross section and angle-resolved light scattering intensity and linear polarization, lead to similar general conclusions (data not shown). Accuracy of C_{abs} versus discretization parameter for Rayleigh particles are shown in Fig. 5 for all considered shapes, refractive indices, and DDA formulations. Analogous results for large particles are shown in Fig. 6. The leftmost points on these figures correspond to estimated extrapolation errors. The minimum of these values among different DDA formulations for the same particle corresponds to the estimated accuracy of the reference result (except for spheres). Therefore, all shown values are expected to have this uncertainty.

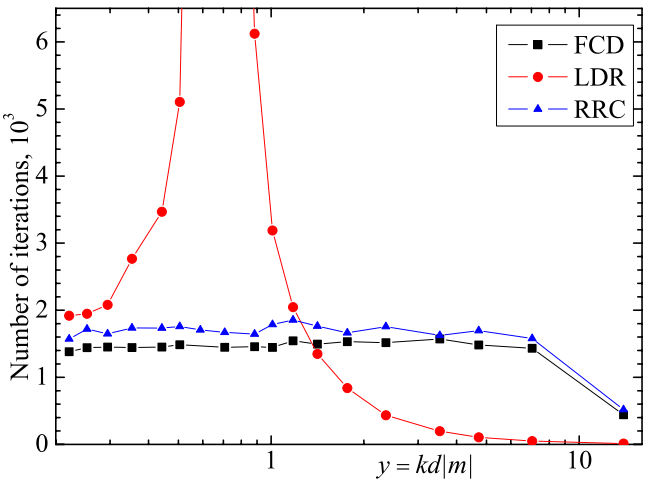

FIG. 4. (Color online) Number of iterations versus y for $kD_x=8$ sphere with $m=10+10i$.

In most cases this uncertainty is negligibly small. The only exception is the GRF4 particle (both Rayleigh and large) for $m=0.1+i$ and $1.6+0.01i$ [see Figs. 5(b), 5(c), 6(d), and 6(f)]. Also in several other cases the errors of the FCD are smaller than the estimated errors of the reference results. In particular, FCD results for the Rayleigh cube [Fig. 5(b)] are probably affected by the value of the default threshold of the iterative solver (10^{-5}). However, in all these cases both mentioned errors are so small that corresponding uncertainty do not affect any of the following conclusions.

The overall tendency is that the FCD is more accurate than other DDA formulations (exceptions are discussed below), but its convergence with decreasing discretization parameter is less regular. The convergence behavior of the FCD is largely unknown. In particular, it is the only DDA formulation, for which the convergence has not been rigorously proven neither in [17] nor, to the best of our knowledge, anywhere else. From a practical viewpoint, oscillations around the linear trend in log-log scale [e.g., Figs. 6(c) and 6(d)] cause relatively large errors during extrapolation of its results. Probably, a modification of the extrapolation technique to account for unusual convergence of the FCD may

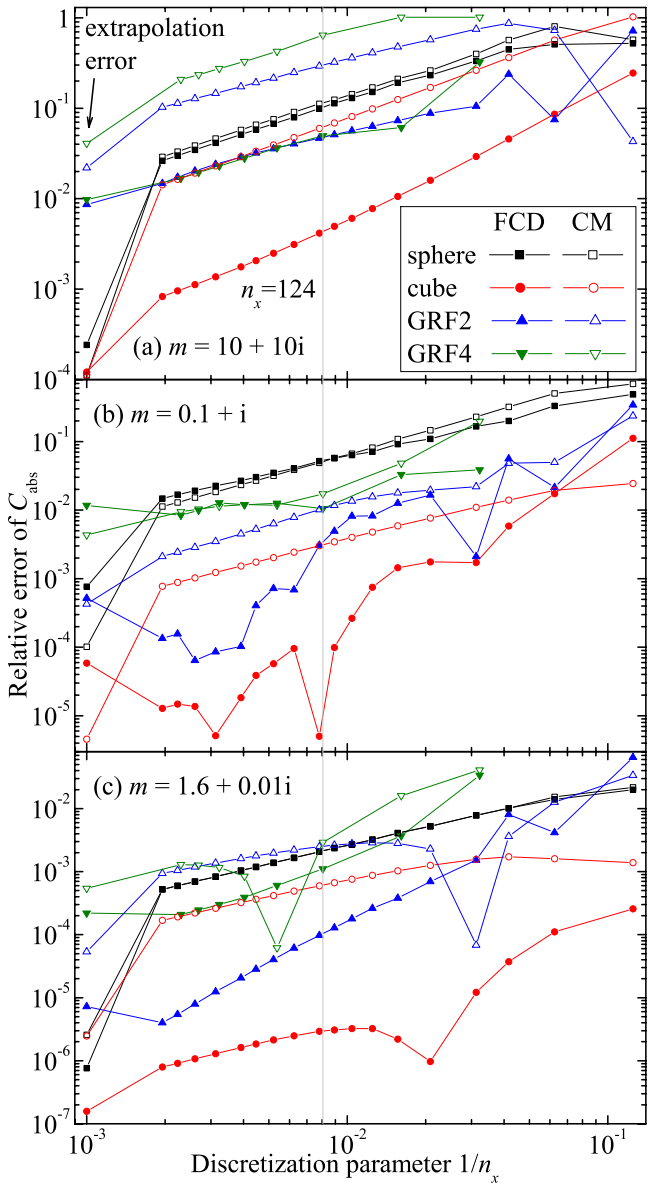

FIG. 5. (Color online) Relative error of C_{abs} versus the discretization parameter for Rayleigh particles in log-log scale. The leftmost points (corresponding to abscissa values of 10^{-3}) show extrapolation errors (real errors for spheres and corrected estimates for other shapes). Gray vertical lines correspond to n_x=124.

improve the quality of the extrapolation. We consider good accuracy of single DDA simulations to be more important than good potential for extrapolation, especially considering the lack of robustness for the latter. Moreover, such oscillatory behavior is not an exclusive feature of the FCD. In particular, similar oscillations were noted for a red blood cell when using the LDR [27].

Another feature of the computations is that convergence is generally nonmonotonic for all DDA formulations. This behavior is exhibited, in particular, by gaps caused by the sign change of errors and complicates adequate comparison between the DDA formulations. Therefore, we propose the maximum error over all simulations with $n_x \geq 124$ as the accuracy measure. It is based on the region of n_x, where convergence is on average monotonic, and diminishes the effect of single gaps. Values of this error measure for all studied cases are shown in Table II.

The following conclusions can be deduced from this table (as well as from data on Figs. 5 and 6). For Rayleigh spheres accuracy of the FCD and the CM is almost the same. For all other cases with $m=10+10i$ the FCD accuracy is 3 to 30 times better than that of the RR (or the CM). Errors of the LDR for large particles with this refractive index are unacceptably large. For $m=0.1+i$ the LDR and the RR result in almost the same accuracy, except for difference for $kD_x=8$ cubes which is due to crossing of zero of the RR error [see Fig. 6(c)]. For all Rayleigh particles with this m the FCD is not worse than the CM, and even 30 times more accurate for the cube. However, for large particles the FCD can be either 3 times more accurate or 4 times less accurate than the RR.

For $m=1.6+0.01i$ the LDR is on average more accurate than the RR, which agrees with Draine *et al.* [2,4]. Moreover, it seems to be widely accepted that there is no large difference between different DDA formulations for such moderate refractive indices. This makes the FCD results especially surprising. For Rayleigh cubically shaped particles (i.e., all except spheres) the FCD was from 3 to 200 times more accurate than the CM. For larger particles the FCD was also clearly superior, improving the accuracy from 1.7 to 6 times in comparison with the LDR (the smallest improvement was for spheres). As far as we know, this feature of the FCD was never observed in the literature, which is probably because this formulation was never systematically applied to cubically shaped particles.

Another important factor is the scaling of errors with refining discretization. Although nonmonotonic convergence significantly complicates the analysis, our wide range of discretization parameters allows drawing the following conclusions. Errors of C_{abs} for the LDR and the RR converge linearly with y or $1/n_x$ for all particles studied, while the FCD leads to significantly faster (approximately quadratic) convergence in some cases. This feature is especially prominent for large cubes with $m=10+10i$ and $1.6+0.01i$ [Figs. 6(a) and 6(e)]. For Rayleigh cubes the linear part of errors is also small, becoming important only for small values of $1/n_x$ (exact values depend on m—Fig. 5). Quadratic convergence is also obtained for the GRF2 with $m=1.6+0.01i$ [Figs. 5(c) and 6(f)].

The differences between shapes can be generalized as follows. Improvement by using the FCD is the least pronounced for spheres, which is discussed in the next subsection. Among cubical shapes, the cube corresponds to the largest improvement (both in values and scaling exponents), then the GRF2, and finally the GRF4 (although this general order is not strict). This order corresponds to increasing surface-to-volume ratio and hence relative importance of surface errors of the DDA. Therefore, we conclude that the FCD is most effective in decreasing the part of discretization errors associated with dipoles far from the surface. However, the efficient susceptibility filtering (see Sec. II B) may improve the efficiency of the FCD for dipoles near the surface as well.

C. Structure of errors for the spheres

To analyze the difference between the spheres and other shapes, we divided the relative errors of C_{abs} for the spheres

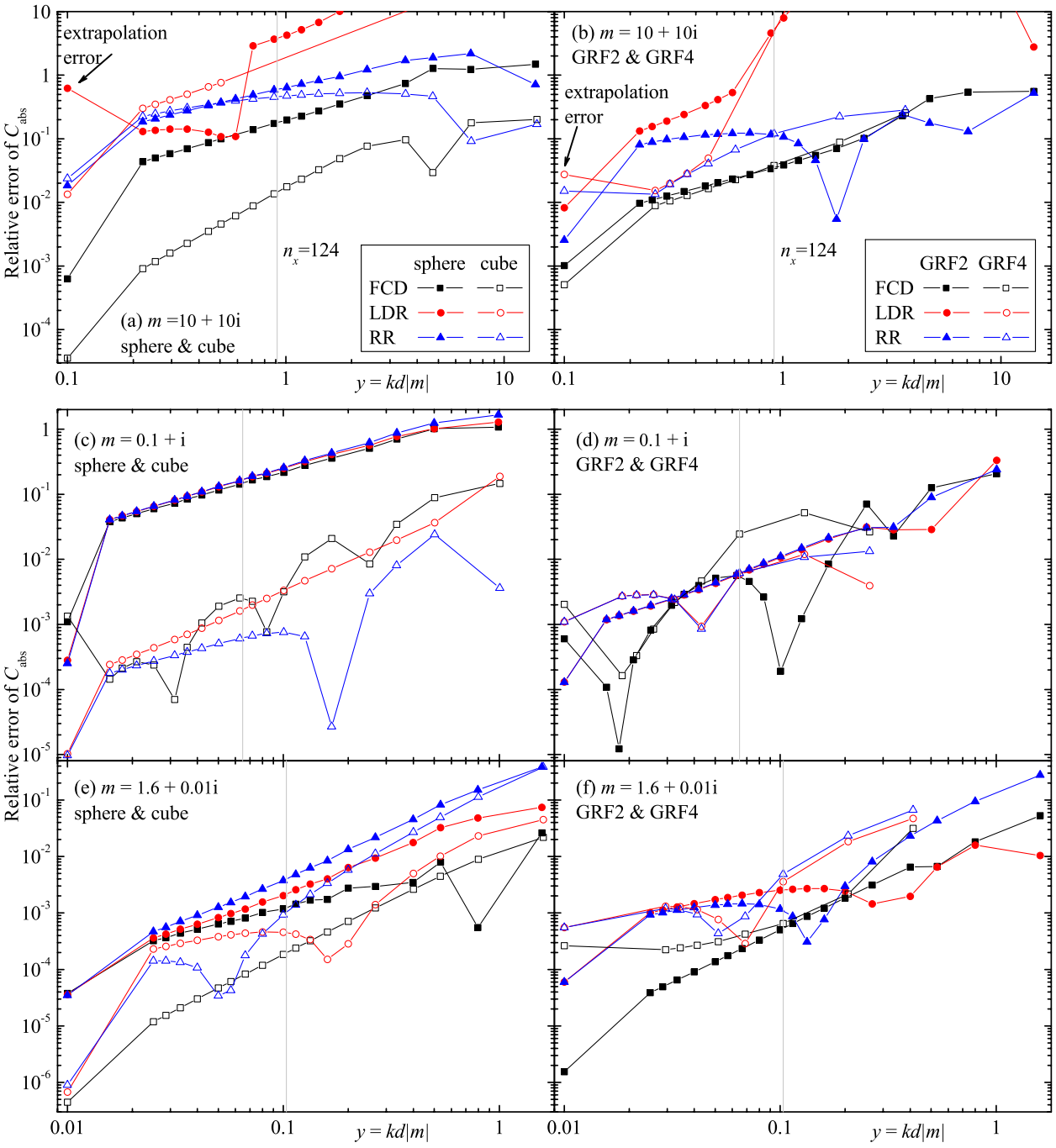

FIG. 6. (Color online) Same as Fig. 5 but for large particles. Left column shows results for spheres and cubes, right—for GRF2 and GRF4 particles. For m=10+10i part of LDR simulations either did not converge (missing data points) or resulted in huge errors (more than ten times).

into shape and discretization parts (as described in Sec. II D). Corresponding results are presented in Fig. 7. We remind the reader that the errors for any sphere, shown in Figs. 5 or 6, are the sum (or difference, depending on relative signs) of the shape and discretization error for the same sphere and DDA formulation. Shape errors are approximately linearly proportional to discretization parameter (slope close to 1 in log-log scale) in agreement with theoretical predictions of [17]. However, this convergence is not expected to be always monotonic, especially for relatively large discretization parameters, as exemplified by Fig. 7(f). This can be partly explained by nonmonotonic dependence of surface irregularity of the dipole grid (e.g., as defined by Draine [3]) on n_x. The same applies to discretization errors [see points with y=0.5 in Fig. 7(d)]. The values of shape errors are generally comparable to the discretization errors, which smoothes the difference between the DDA formulations when looking at total instead of discretization errors.

For large particles difference between the DDA formulations for discretization errors of spheres correlates with that

TABLE II. Maximum for all $n_x \geq 124$ relative error of C_{abs}.

		$kD_x \ll 1$		$kD_x = 8$		
m	Shape	CM	FCD	RR	LDR	FCD
$10+10i$	Sphere	0.11	0.10	0.58	3.7	0.17
	Cube	0.060	0.0042	0.45	[a]	0.014
	GRF2	0.29	0.047	0.12	4.6	0.034
	GRF4	0.64	0.050	0.12	[a]	0.038
$0.1+i$	Sphere	0.049	0.052	0.16	0.16	0.14
	Cube	0.0030	9.6×10^{-5}	6.1×10^{-4}	0.0016	0.0025
	GRF2	0.010	0.0031	0.0059	0.0058	0.0056
	GRF4	0.017	0.013	0.0061	0.0059	0.024
$1.6+0.01i$	Sphere	0.0021	0.0021	0.0038	0.0020	0.0012
	Cube	5.9×10^{-4}	2.9×10^{-6}	9.3×10^{-4}	4.6×10^{-4}	1.8×10^{-4}
	GRF2	0.0025	9.8×10^{-5}	0.0015	0.0025	5.0×10^{-4}
	GRF4	0.0029	0.0011	0.0049	0.0036	5.8×10^{-4}

[a]The method failed to converge within 30 000 iterations at least for one value of $n_x \geq 124$.

of cubes. For $m=0.1+i$ this difference is small for both spheres and cubes, while for other two m using the FCD leads to significant decrease of discretization errors for both shapes. However, there is no such correlation for Rayleigh particles because the FCD do not show considerable improvement of discretization errors for Rayleigh spheres. Moreover, in all cases discretization errors for spheres converge linearly and are much larger than that for cubes.

It is tempting to conclude that surface errors (the part of discretization errors, converging linearly, see Sec. II D) for spheres are much larger than those for cubes. However, the points on any chosen curve of discretization errors in Fig. 7 are not for the same particle, but for slightly different discretizations of the same sphere. Therefore, theoretical conclusions from [17], in particular the association of surface errors with the linear part of the convergence curve, do not apply. To assess surface errors unambiguously one may study convergence of errors with increasing n_x for fixed initial discretized shape, which is an extended version of simulations that were used to estimate accurate results for these discretized shapes through extrapolation. Such comprehensive study is outside the scope of this paper. However, our preliminary simulations in this direction resulted in power-law convergence with exponent values between 1 and 2 (data not shown).

For now, we conclude that the concept of surface error has limited applicability to noncubically shaped particle. Therefore, the main conclusion of this subsection is that (total) discretization errors of the FCD for spheres are markedly different from that for the cubes. As a plausible explanation we suggest that the FCD is sensitive not only to the surface-to-volume ratio (which is approximately the same for this two shapes) but also to ratio of characteristic surface scale to dipole size. In other words, the FCD is more accurate when dipole set can be divided into large cubical homogeneous quasidipoles. This is intuitively understandable considering the sampling nature of the FCD. Another possible explanation is discussed in Sec. IV.

D. Computational time

For practical applications one is usually interested not in accuracy for fixed discretization, but in required discretization and computational time to obtain this desired accuracy. We choose a typical accuracy goal, 10% relative error of C_{abs}, but require it to be fulfilled not only for a single value of n_x, but for all n_x larger than some threshold value. This is done to decrease the influence of nonmonotonic convergence. Computational times corresponding to those threshold values of n_x for different problem parameters are shown in Table III.

For $m=10+10i$ using the FCD decreases the computational time by several orders of magnitude, which is a combination of decreasing number of iterations and improving accuracy. This makes such extreme refractive indices, in principle, feasible for DDA simulations, although the simulation times can be large (about 1 processor hour). For $m=0.1+i$ the FCD is slightly faster for Rayleigh particles and comparable to other formulations for $kD_x=8$, which agrees with the accuracy results. Computational times for $m=1.6+0.01i$ are almost the same for all DDA formulations, because in most cases required accuracy is achieved using the minimum tested value of n_x. Therefore, these values do not reflect the observed superiority of the FCD in accuracy for this m.

We also note that computational times for the cubes are smallest among all shapes (especially for $m=10+10i$), while for the spheres they are largest (especially for $m=0.1+i$). This is a direct implication of the difference of DDA accuracy between particle shapes, discussed above.

IV. SPECTRAL PROPERTIES

We finally examine the special case of Rayleigh homogeneous scatterers and present a short introduction into the spectral representation formalism, following [28,29]. In this case $x=0$, $M=0$ [cf. Eqs. (4) and (9)], and hence α is that of

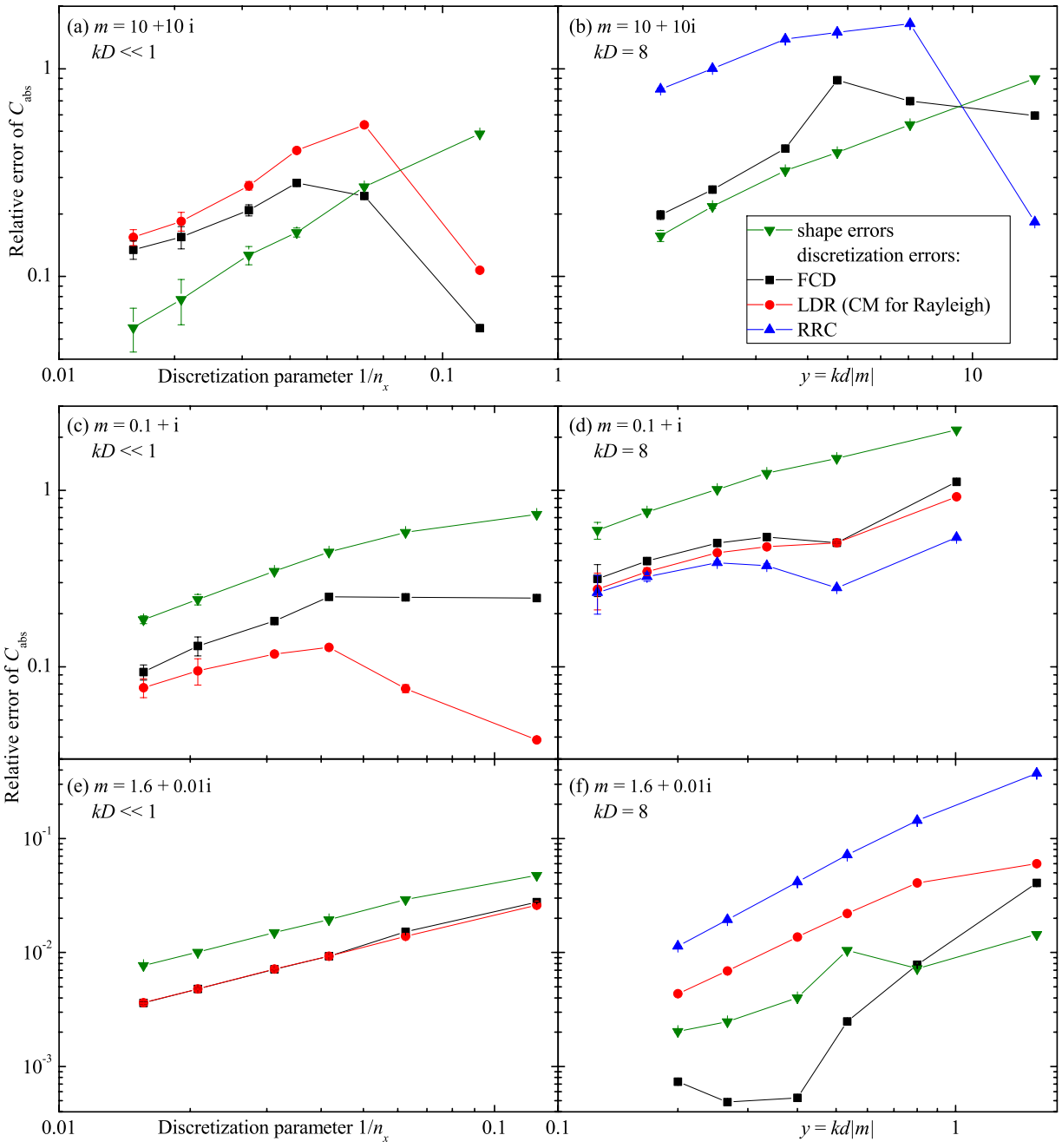

FIG. 7. (Color online) Shape and discretization parts of relative errors of C_{abs} for the spheres in log-log scale. Left and right columns show results for Rayleigh and large sizes respectively. Error bars are due to uncertainties of the reference results for cubical discretizations of the spheres, calculated by the extrapolation technique. For most data the error bars are narrower than the symbol width. In figure part (b) discretization errors of the LDR are not shown because they are larger than 10. In figure part (f) nonmonotonic behavior of FCD results is due to sign change.

the CM. Moreover, the Green's tensor is purely real [cf. Eqs. (2) and (7)]. We rewrite Eq. (5) in matrix form as

$$\mathbf{BE} = \chi(z\mathbf{I} - \mathbf{W})\mathbf{E} = \mathbf{E}^{\text{inc}}, \quad z = V\alpha^{-1} = \frac{4\pi}{3}\frac{\varepsilon + 2}{\varepsilon - 1}, \quad \mathbf{W} = V\mathbf{G}, \tag{10}$$

where $\mathbf{E}$ and $\mathbf{E}^{\text{inc}}$ are arrays combined from $\mathbf{E}_i$ and $\mathbf{E}_i^{\text{inc}}$ respectively for all dipoles, $\mathbf{I}$ is the identity matrix, and matrix $\mathbf{G}$ contains the values of Green's tensor and has zero diagonal. z and χ contains all information about material properties, while $\mathbf{W}$ describes the shape of the scatterer. $\mathbf{W}$ is real-symmetric and $\mathbf{B}$ is Hermitian contrary to the non-Rayleigh case, when both these matrices are complex-symmetric. Finding the spectrum of $\mathbf{W}$ (set of real values w_n) and diagonalizing this matrix, one can easily solve Eq. (10) for many different values of ε. We stress that this spectrum, discussed in detail below, is completely different from the spatial spec-

TABLE III. Computational time (processor seconds) to provide persistent accuracy of C_{abs} at least 10%.[a]

		$kD_x \ll 1$		$kD_x=8$		
m	Shape	CM	FCD	RR	LDR	FCD
$10+10i$	Sphere	2×10^4	2000	$>3\times10^6$	$>4\times10^6$	3×10^5
	Cube	3000	1	$>7\times10^6$	$>8\times10^6$	200
	GRF2	8×10^5	40	1×10^6	$>2\times10^6$	1000
	GRF4	$>1\times10^6$	500	3×10^5	1×10^6	7000
$0.1+i$	Sphere	700	200	3×10^4	3×10^4	2×10^4
	Cube	0.4	2	0.6	3	3
	GRF2	2	2	2	2	8
	GRF4	500	30	40	40	40
$1.6+0.01i$ [b]	Sphere	0.1	0.1	3	0.2	0.3
	Cube	0.1	0.1	5	0.3	0.4
	GRF2	0.2	0.2	0.8	0.3	0.3
	GRF4	6	7	10	10	10

[a]Accuracy of the shown estimates is between one significant digit and an order of magnitude due to the large step in values of n_x and varying number of Intel Xeon 3.4 GHz processors that were used in simulations.
[b]For this m we used convergence threshold of the iterative solver equal to 10^{-10}, therefore shown time values are approximately twice as large as for the default threshold of 10^{-5}.

trum, used in the derivation of the FCD (Sec. II B).

One of the most often considered optical property of the Rayleigh scatterers is its absorption cross-section C_{abs} normalized by the scatterer volume V_s. Moreover, usually the scatterer is considered in random orientation leading to [28]

$$\frac{\langle C_{abs}\rangle}{kV_s} = 4\pi\,\mathrm{Im}\sum_n \frac{f_n}{z-w_n} = \mathrm{Im}\sum_n \frac{f_n}{1/(\varepsilon-1)+v_n} = \mathrm{Im}\int \frac{f(v)\mathrm{d}v}{1/(\varepsilon-1)+v}, \quad (11)$$

where $v_n=1/3-w_n/4\pi$ are generalized depolarization factors (in analogy to ellipsoids, or form-factors [29]) and f_n are real weights computed from the corresponding eigenvectors of $\mathbf{W}$. Therefore, for the purpose of computing $\langle C_{abs}\rangle$ the shape of the scatterer is fully characterized by sets $\{w_n,f_n\}$ or $\{v_n,f_n\}$, or equivalently by function $f(v)$. Those sets are called density of states and distribution of depolarization factors (or form-factors), respectively [28]. To compute other measured quantities one should consider several sets of weights, corresponding to the polarizability tensor of the whole particle [29], but we do not analyze them here.

To generalize this approach one may look at Eq. (10) as a discretization of a corresponding infinite-dimensional operator equation, obtained by replacing vectors by functions and matrices by linear operators. Set of w_n is then a certain approximation to the spectrum of operator $\mathbf{W}$ and $\Sigma f_n\delta(v-v_n)$ is an approximation to $f(v)$. The DDA is not the only method to compute these estimates. For instance, discretization of the surface-integral equation [30,31] or multipole expansion [32,33,28] can be used, all leading to the same result. Other notable examples are the DDA applied to clusters of spheres with each sphere described by a single dipole [34] and attempts to extend this approach to non-Rayleigh scatterers [35].

Budko and Samokhin [36] rigorously proved that the spectrum of the operator $\mathbf{W}$ is bounded between $-8\pi/3$ and $4\pi/3$ (corresponding to form factors between 0 and 1), which was also justified using physical arguments by Rahola [37] and Markel *et al.* [28]. In the latter paper it was also stated that the spectrum should lie strictly *inside* the specified bounds. However, any finite-dimensional approximation $\{w_n\}$ is only expected to converge to the operator spectrum with increasing n. Although numerical tests [29,37] showed that values of w_n approximately fall into the specified bounds, strict compliance do not necessarily take place for any finite n.

We computed the form-factor distributions for the GRF2 particle, using both the FCD and the CM and different levels of discretizations (number of dipoles N_{dip} is from 100 to 6400). Since the total number of eigenvalues $N_{eig}=3N_{dip}$, presenting the whole set $\{v_n,f_n\}$ or the function $\Sigma f_n\delta(v-v_n)$ is not practical. We have smoothed the latter to produce a piecewise linear function, each point of which is obtained by averaging over $\sqrt{N_{eig}}$ eigenvalues. In comparison with replacing delta functions with Lorentz profiles [28], this approach improves the resolution of $f(v)$ in regions of high density of eigenvalues (e.g., near $v=0$ and 1) and preserves the support of $f(v)$, i.e., limiting bounds of v. Resulting smoothed distributions are shown in Fig. 8.

Form-factor distributions computed using different formulations of the DDA seem to converge to the same function with refining discretization. Moreover, there is not so large difference between the results for $N_{dip}\geq 800$, which suggests that we caught all main features of the "true" $f(v)$. However, there is an important difference between the results for the

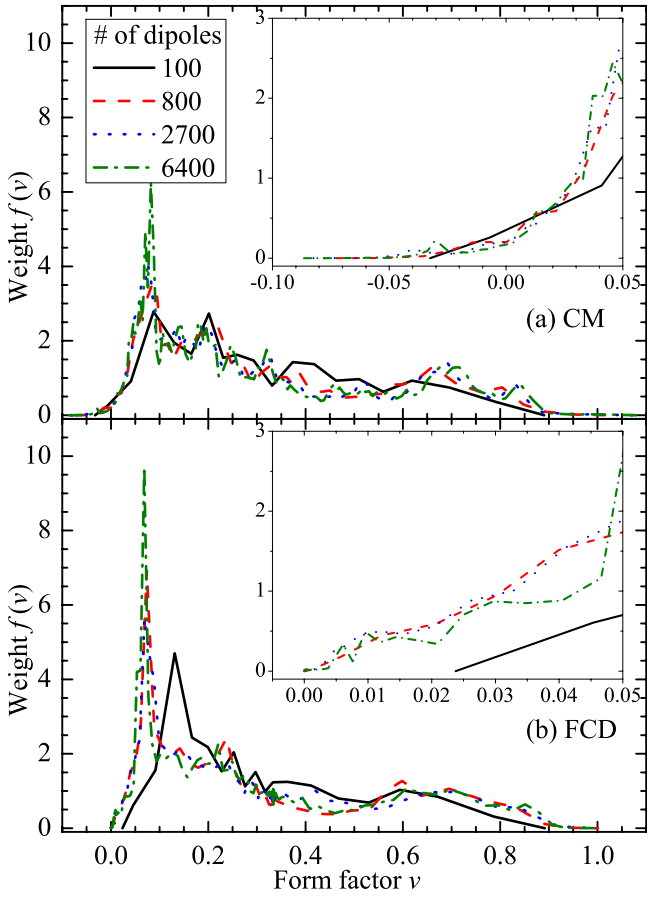

FIG. 8. (Color online) Form-factor distributions for GRF2 particle, computed using the CM (a) and the FCD (b). Results are obtained by smoothing (see text) from sets $\{v_n, f_n\}$ obtained for several levels of discretization. Insets show detailed behavior near zero values of v.

CM and the FCD. The form-factors for the FCD are always between 0 and 1 (within the numerical errors of eigenvalues calculation—smaller than 10^{-5}), while that for the CM fall out of this range (to a lesser extent for finer discretizations). We hypothesize that this is a general feature of the FCD, although a prove is not readily available.

This difference at the side-tails of $f(v)$ may seem not that large when compared to the middle of the distributions. However, inspection of Eq. (11) readily reveals that values of $f(v)$ near $v=0$ and $v=1$ determine the absorption for $|\varepsilon| \gg 1$ and $|\varepsilon| \ll 1$, respectively. In particular, this explains better performance of the FCD for $m=10+10i$ ($\varepsilon=200i$). Moreover, Eq. (11) leads to resonant behavior for $\varepsilon=1-1/v$. For $0<v<1$ these resonances are located on *negative* real axis, but may shift to the *positive* real axis, when v fall out of this bounds. For instance, significant nonzero values of $f(v)$ near $v=-0.01$ [Fig. 8(a)] should lead to very inaccurate results (breakdown) of the CM formulation for $\varepsilon \approx 100$ ($m \approx 10$). We leave numerical verification of this fact for future research, but note that it also explains very slow convergence of the iterative solver in the CM formulation for large real refractive indices, mentioned in Sec. III A.

In contrast, consider another studied value of $m=0.1+i$ ($\varepsilon=-0.99+0.2i$). It is located near resonance corresponding to $v=0.5$, where there is no significant differences between $f(v)$ calculated with the CM and the FCD. This explains why FCD leads to relatively small improvement (if any) both in accuracy and convergence of iterative solver compared to the CM for this m.

As stated above form-factor distribution is completely determined by the scatterer shape. In particular, there exist analytical solution for a sphere $f(v)=\delta(v-1/3)$, which transforms to narrow distributions around $v=1/3$ by discretization using both the CM and the FCD (data not shown). This narrow distributions lack "resonant" regions of v (near 0 and 1) and hence superiority of the FCD in these regions becomes less relevant. This makes a sphere (as well as general ellipsoids, characterized by three delta functions) markedly different from other shapes, which form-factor distributions covers the whole range from 0 to 1 (data not shown). Therefore, we propose these form-factor distributions as a possible explanation of difference in improvement of the DDA accuracy by using the FCD between a sphere and other shapes. However, more shapes (both cubical and noncubical) should be studied to make any conclusions.

Although the above is based on the assumption of Rayleigh sizes, the ideas presented may explain many results for larger scatterers, especially with respect to accuracy of DDA simulations.

V. CONCLUSION

We have compared three DDA formulations: the FCD, the LDR, and the RR for simulations of light scattering by cubes, spheres, and GRF particles with sizes comparable and much smaller than the wavelength, using three refractive indices: $10+10i$, $0.1+i$, and $1.6+0.01i$.

The FCD improves convergence of the iterative solver for Rayleigh particles with extreme refractive indices: it is about 6 and 1.2 times faster than CM for $m=10+10i$ and $0.1+i$, respectively. Also the FCD is from 3 to 30 times more accurate than the RR in calculation of C_{abs} for nonspherical particles with $m=10+10i$. For $m=0.1+i$ all studied formulations lead to similar results, but FCD was 30 times more accurate for Rayleigh cubes. Surprisingly, even for moderate $m=1.6+0.01i$ the FCD was from 3 to 200 times more accurate than the LDR for all nonspherical shapes. Overall, using the FCD allows one to decrease the computational time to reach a prescribed accuracy by up to several orders of magnitude. The only drawback of FCD is that in some cases the extrapolation technique applied to its results leads to larger errors than for other formulations. If comparing the LDR and the RR, our results show that the LDR is a "never use" option for $m=10+10i$, comparable to the RR (and generally to FCD) for $m=0.1+i$, and better than the RR for $1.6+0.01i$.

To get insight about the difference in performance between different DDA formulations and particle shapes, we analyzed the detailed structure of DDA errors and the spectrum of the DDA interaction matrix. In particular, so-called discretization errors of the FCD for spheres are markedly different from that for the cubes, which suggests that the

FCD is sensitive to characteristic surface scale of the cubical discretization of the particle. We empirically showed that discretization of the integral scattering operator (in the Rayleigh regime) using the FCD retains the limiting bounds of its spectrum, in contrast to the CM formulation. This explains better performance of the FCD for large $|m|$. We also conclude that a spherical shape is a very special case for the DDA, hence other shapes must be examined in any study of the DDA accuracy.

The FCD has been implemented in the publicly available code ADDA and is ready to be applied by the light scattering community. Although further comparative studies are definitely required, the FCD is at least a very good candidate to become a default DDA formulation for day-to-day simulations. Extreme refractive indices, such as considered in this paper, can be routinely (although not quickly) simulated using modern desktop computers.

ACKNOWLEDGMENTS

We thank Patrick C. Chaumet for illuminating discussion on application of different DDA formulations to particles with real refractive index and anonymous reviewer for useful comments. This research is supported by program of the Russian Government "Research and educational personnel of innovative Russia" (Contract No. P2497). Ma.Y. is also supported by grants of the Siberian Branch of the Russian Academy of Science (Grants No. 2009-37 and No. 2009-7), program of Presidium of the Russian Academy of Science (Grant No. 2009-27-15), and by grant from Carl Zeiss for young scientists of leading Russian universities.

[1] M. A. Yurkin and A. G. Hoekstra, J. Quant. Spectrosc. Radiat. Transf. **106**, 558 (2007).
[2] B. T. Draine and J. J. Goodman, Astrophys. J. **405**, 685 (1993).
[3] B. T. Draine, Astrophys. J. **333**, 848 (1988).
[4] B. T. Draine and P. J. Flatau, J. Opt. Soc. Am. A **11**, 1491 (1994).
[5] A. C. Andersen, H. Mutschke, T. Posch, M. Min, and A. Tamanai, J. Quant. Spectrosc. Radiat. Transf. **100**, 4 (2006).
[6] P. B. Johnson and R. W. Christy, Phys. Rev. B **6**, 4370 (1972).
[7] T. Henning and R. Stognienko, Astron. Astrophys. **311**, 291 (1996).
[8] A. Laor and B. T. Draine, Astrophys. J. **402**, 441 (1993).
[9] J. L. Servoin and B. Piriou, Phys. Status Solidi B **55**, 677 (1973).
[10] F. Kemper, A. de Koter, L. B. F. M. Waters, J. Bouwman, and A. G. G. M. Tielens, Astron. Astrophys. **384**, 585 (2002).
[11] N. B. Piller and O. J. F. Martin, IEEE Trans. Antennas Propag. **46**, 1126 (1998).
[12] N. B. Piller, Opt. Lett. **22**, 1674 (1997).
[13] P. C. Chaumet, A. Sentenac, and A. Rahmani, Phys. Rev. E **70**, 036606 (2004).
[14] A. Rahmani, P. C. Chaumet, and G. W. Bryant, Opt. Lett. **27**, 2118 (2002).
[15] A. Rahmani, P. C. Chaumet, and G. W. Bryant, Astrophys. J. **607**, 873 (2004).
[16] M. J. Collinge and B. T. Draine, J. Opt. Soc. Am. A **21**, 2023 (2004).
[17] M. A. Yurkin, V. P. Maltsev, and A. G. Hoekstra, J. Opt. Soc. Am. A **23**, 2578 (2006).
[18] M. A. Yurkin, V. P. Maltsev, and A. G. Hoekstra, J. Quant. Spectrosc. Radiat. Transf. **106**, 546 (2007).
[19] N. B. Piller, Opt. Commun. **160**, 10 (1999).
[20] M. A. Yurkin, M. Min, and A. G. Hoekstra, in *Proceedings of the 11th Conference on Electromagnetic and Light Scattering* (University of Hertfordshire, Hatfield, UK, 2008), pp. 109–112.
[21] M. A. Yurkin, D. de Kanter, and A. G. Hoekstra, J. Nanophotonics **4**, 041585 (2010).
[22] M. Min, L. B. F. M. Waters, A. de Koter, J. W. Hovenier, L. P. Keller, and F. Markwick-Kemper, Astron. Astrophys. **462**, 667 (2007).
[23] P. Gay-Balmaz and O. J. F. Martin, Comput. Phys. Commun. **144**, 111 (2002).
[24] http://code.google.com/p/a-dda/ (2010).
[25] https://subtrac.sara.nl/userdoc/wiki/lisa/description (2010).
[26] M. A. Yurkin, V. P. Maltsev, and A. G. Hoekstra, J. Opt. Soc. Am. A **23**, 2592 (2006).
[27] K. V. Gilev, E. Eremina, M. A. Yurkin, and V. P. Maltsev, Opt. Express **18**, 5681 (2010).
[28] V. A. Markel, V. N. Pustovit, S. V. Karpov, A. V. Obuschenko, V. S. Gerasimov, and I. L. Isaev, Phys. Rev. B **70**, 054202 (2004).
[29] M. Min, J. W. Hovenier, A. Dominik, A. de Koter, and M. A. Yurkin, J. Quant. Spectrosc. Radiat. Transf. **97**, 161 (2006).
[30] R. Fuchs, Phys. Rev. B **11**, 1732 (1975).
[31] C. Pecharromá, J. Perez-Juste, G. Mata-Osoro, L. M. Liz-Marzan, and P. Mulvaney, Phys. Rev. B **77**, 035418 (2008).
[32] D. Langbein, J. Phys. A **9**, 627 (1976).
[33] R. Rojas and F. Claro, Phys. Rev. B **34**, 3730 (1986).
[34] V. A. Markel, L. S. Muratov, M. I. Stockman, and T. F. George, Phys. Rev. B **43**, 8183 (1991).
[35] V. A. Markel, V. M. Shalaev, E. B. Stechel, W. Kim, and R. L. Armstrong, Phys. Rev. B **53**, 2425 (1996).
[36] N. V. Budko, A. B. Samokhin, and A. A. Samokhin, Diff. Eq. **41**, 1262 (2005).
[37] J. Rahola, SIAM J. Sci. Comput. (USA) **21**, 1740 (2000).
[38] Laboratory of Paper Coating and Converting at Åbo Akademi University, http://albin.abo.fi/~jkniivil/litebil (2010).